Earth and Planetary Science Letters 286 (2009) 230–242

Contents lists available at ScienceDirect

Earth and Planetary Science Letters

journal homepage: www.elsevier.com/locate/epsl

Iron-oxidizing microbial ecosystems thrived in late Paleoproterozoic redox-stratified oceans

Noah Planavsky [a,b,*], Olivier Rouxel [b], Andrey Bekker [c], Russell Shapiro [d], Phil Fralick [e], Andrew Knudsen [f]

[a] Department of Earth Sciences, University of California, Riverside, 900 University Ave., Riverside, CA, 92521, USA
[b] Department of Marine Chemistry and Geochemistry, Woods Hole Oceanographic Institute, MS25, 266 Woods Hole Road, Woods Hole, MA 02543, USA
[c] Department of Geological Sciences, University of Manitoba, Winnipeg, MB, Canada R3T 2N2
[d] Department of Geological and Environmental Sciences, California State University, Chico, Chico, CA 95929, USA
[e] Department of Earth Sciences, Lakehead University, 955 Oliver Road, Thunder Bay, ON, Canada P7B 5E1
[f] Geology Department, Lawrence University, P.O. Box 599, Appleton, WI, 54912, USA

ARTICLE INFO

Article history:
Received 23 September 2008
Received in revised form 19 June 2009
Accepted 23 June 2009
Available online 5 August 2009

Editor: M.L. Delaney

Keywords:
iron-bacteria
iron-formations
Fe-isotopes
rare earth elements
Paleoproterozoic
stromatolites

ABSTRACT

We conducted a geochemical and petrographic study of the 1.89 billion year old Gunflint and Biwabik iron formations, with the goal of determining the importance of microbial iron-oxidation in the formation of iron- and microfossil-rich stromatolites. We used redox-sensitive tracers, such as iron isotopes and rare earth elements, to decipher whether these ancient microbial ecosystems harbored cyanobacteria or Fe-oxidizing bacteria as primary producers. Iron-rich stromatolites contain non-significant or positive Ce anomalies, which contrast with shallow water deposits having negative Ce anomalies. This trend in Ce anomalies indicates that the stromatolites formed in low oxygen conditions, which is the ideal setting for the proliferation of Fe-oxidizing bacterial ecosystems. The stromatolites yield a large range of δ^{56}Fe values, from −0.66 to +0.82‰, but contain predominantly positive values indicating the prevalence of partial Fe-oxidation. Based on modern analogues, Fe-oxides precipitated in cyanobacterial mats are expected to record an isotopic signature of quantitative oxidation, which in marine settings will yield negative δ^{56}Fe values. The stromatolite iron isotope data, therefore, provide evidence for the presence of Fe-oxidizing bacteria. The stromatolites can be traced for a distance of over 100 km in these iron formations, indicating that they record a pervasive rather than localized ecosystem. Their preservation in late Paleoproterozoic successions deposited along the margins of the Superior craton suggests that there was a global expansion of iron-oxidizing bacterial communities at shallow-water redox boundaries in late Paleoproterozoic oceans.

1. Introduction

The first detailed descriptions of Precambrian microfossils (Awramik and Barghoorn, 1977; Barghoorn and Tyler, 1965; Cloud, 1965; Strother and Tobin, 1987) established the paradigm that oxygenic photosynthesizers were the dominant primary producers in early Precambrian ecosystems. However, widespread anoxia in the early Precambrian likely allowed the global expansion of chemolithotrophic microbial communities that are now restricted to locally reducing marine environments (Canfield et al., 2006; Kappler et al., 2005; Konhauser et al., 2002). A reducing or weakly oxidizing atmosphere, widespread anoxia, and a small oceanic sulfur reservoir throughout most of Archean and early Paleoproterozoic time, likely allowed H_2 and Fe^{2+}, present in nanomolar concentrations in modern oceans, to attain high enough concentrations to sustain microbial ecosystems in marine settings. Iron oxidizing bacteria have been proposed to be important primary producers in early Precambrian oceans for almost 100 years (Harder 1919), and this idea has been further elaborated upon in a series of recent studies (Johnson et al., 2008; Kappler et al., 2005; Konhauser et al., 2002; Widdel et al., 1993). However, there is still little empirical evidence supporting the presence of this type of ecosystem.

Here, we present a geochemical study of Paleoproterozoic microbial ecosystems captured by stromatolites in the ca. 1.9 Ga Animikie basin iron formations. Our goal is to estimate the importance of microbial Fe-oxidation as a means of primary carbon fixation in shallow shelf environments. The Animikie basin in the Lake Superior region contains a well-preserved and depositionally diverse iron-rich sedimentary sequence (Fig. 1), long recognized for providing a wealth of information about early ecosystems. Microfossils from the ~1.9 Ga Gunflint Iron Formation in the Animikie basin were the first discovered indisputable evidence for life on the early Earth and are generally regarded as a benchmark with which to compare other traces of early life (Awramik and Barghoorn, 1977;

* Corresponding author. Department of Earth Sciences, University of California, Riverside, 900 University Ave., Riverside, CA, 92521, USA.
E-mail address: noah.planavsky@email.ucr.edu (N. Planavsky).

0012-821X/$ – see front matter © 2009 Published by Elsevier B.V.
doi:10.1016/j.epsl.2009.06.033

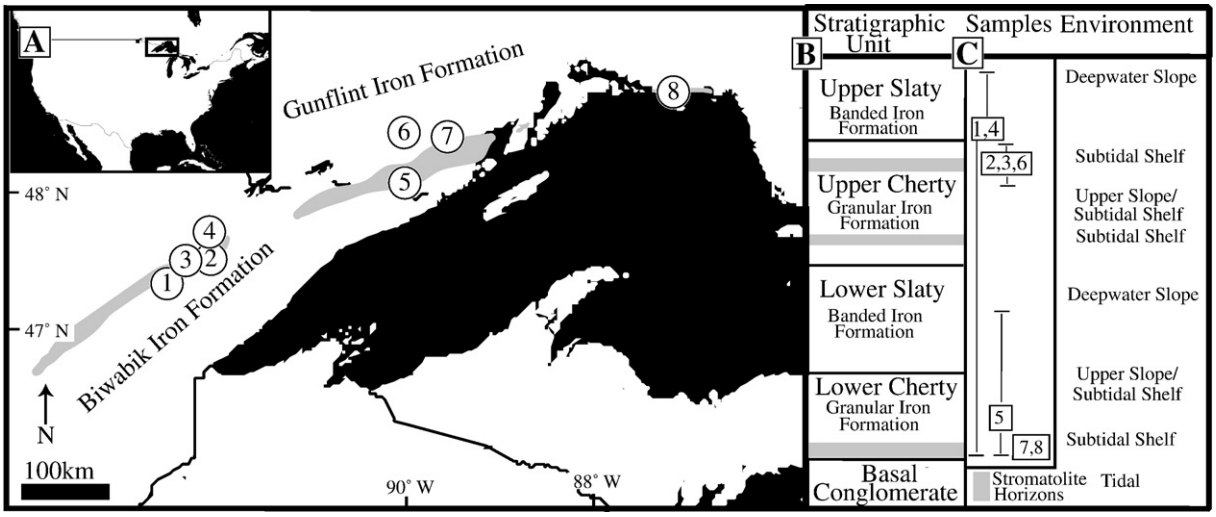

Fig. 1. (A) Location of the outcrops, drill cores, and open-pit iron mines within the Gunflint and Biwabik iron formations that were sampled for this study. The extent of the iron ranges is outlined in grey. (B) Generalized stratigraphy of the iron formations with divisions for the Biwabik Iron Formation; stromatolite horizons are marked by the grey pattern. Stromatolite horizons range in thickness from 1 to 8 m. (C) Stratigraphic range and depositional environment of studied outcrop and drill core sections. Information on the depositional facies model and correlations within the Animikie basin are found in Ojakangas et al. (2001). Locality information is listed in Appendix A.

Barghoorn and Tyler, 1965; Cloud, 1965; Knoll, 2003). Despite extensive study of the Gunflint microfossils, interpretations of the basic ecosystem structure in the Gunflint and correlative iron formations of the Animikie basin are still disputed. Notably, there are disparate interpretations on the presence or importance of Fe-oxidizing bacteria (e.g. Awramik and Barghoorn, 1977; Barghoorn and Tyler, 1965; Cloud, 1965; Knoll, 2003; Knoll and Simonson, 1981; Strother and Tobin, 1987). Previous reconstructions of ecosystem structure in the Animikie basin iron formations are based largely on microfossil morphologies, and the difference in interpretations undoubtedly stems from the difficulty in linking simple microfossils with a specific metabolism based on morphology alone. In this paper we focus on the stromatolitic facies of the Animikie basin iron formations and use redox-sensitive proxies, such as iron isotopes and rare earth elements (REEs), to decipher ecosystem structure and paleoenvironmental conditions at ca. 1.9 Ga.

2. Geologic background

2.1. Geological setting of the Animikie basin iron formations

The Paleoproterozoic Animikie basin is located in the Lake Superior region of Canada and the USA and contains several geographically separate but coeval thick, iron-formation-bearing sedimentary successions. The basin extends northeastward from the Mesabi Range (containing the Biwabik Iron Formation) in north-central Minnesota to the Gunflint Range in Ontario (Fig. 1). The Gogebic Iron Range in north-central Wisconsin and the Upper Peninsula of Michigan lies along the eastern extension of the basin (Ojakangas et al., 2001). The age of Animikie iron formations is well constrained by U–Pb zircon ages of associated volcanic and volcaniclastic beds at 1874 ± 9 Ma (southeastern most extension in Michigan; Schneider et al., 2002) and 1878 ± 1.3 Ma (Gunflint Formation; Fralick et al., 2002).

The tectonic model for the Animikie Basin has been debated for many years (Pufahl and Fralick, 2004). Hoffman (1987) proposed the foreland basin model and postulated that it formed in response to crustal loading during the Penokean orogeny. This model has since been expanded upon and modified by Morey and Southwick (1993) and Ojakangas et al. (2001). More recently, a combined approach using geochronology, petrology of synorogenic intrusions, and sedimentology has revitalized the notion that the iron-formations formed in extensional basins north of the subduction zone in the earliest stages of the Penokean orogeny (Fralick et al., 2002; Schulz and Cannon, 2007).

Despite disagreements about the overall tectonic setting, the sedimentary packages in the Gunflint and Mesabi Iron Ranges are time correlative based on sequence stratigraphy and geochronology (Fralick et al., 2002; Ojakangas et al., 2001; Schneider et al., 2002; Schulz and Cannon, 2007). Previous studies recognized that the stratigraphy in the Mesabi Iron Range is best explained by two transgressive–regressive cycles (Ojakangas, 1983; Ojakangas et al., 2001). Lithotypes in the Animikie basin vary along a bathymetric gradient (Ojakangas et al., 2001) from nearshore tidal deposits of sandstone and chert grainstone to deeper-water iron-rich grainstone (cherty/granular iron formations) and thinly-bedded chemical mudstone (slaty/banded iron formations). There are also two extensive units with stromatolites and oncoids associated with grainstones and ferruginous chert (Fig. 1).

Our study focused on extensive and well-preserved successions in the Gunflint and Biwabik Iron Formations (Fig. 1). Samples for geochemical analyses came from drill core, outcrops, and exposures in open pit iron mines (Fig. 1). Regional metamorphic conditions range from prehnite to pumpellyite to lower greenschist facies of metamorphism (French, 1973). The highly metamorphosed sections of the Biwabik iron formation were avoided. Sample and locality information are provided in Table 1 and Appendix A.

2.2. Stromatolites and microfossils in the Animikie basin iron formations

The stromatolites in the Gunflint and Biwabik Iron Formations have variable chemical compositions and morphologies. Stromatolite morphology varies from small columns (~1 cm in diameter) with rare branching to large hemispheroids up to 1 m in diameter (Hofmann, 1969). Petrographic evidence suggests that silica in the siliceous columnar stromatolites was precipitated from seawater (Cloud, 1965; Gross, 1972; Maliva et al., 2005). There are calcitic stromatolites in the Gunflint Iron Formation (Fralick, 1989; Sommers et al., 2000) that appear to have formed in shallow, high-energy setting. The carbonate stromatolites are found at a paleoexposure surface, and it is unresolved whether the calcite is derived from meteoric replacement of a siliceous or siderite matrix, or recrystallization of marine precipitates (Fralick, 1989; Sommers et al., 2000). Some siliceous

Table 1
Sample description and geochemical compositions of samples from the Animikie basin iron formations.

Sample name and locality	Facies type	SiO_2 (wt.%)	Al_2O_3 (wt.%)	Fe_2O_3(T) (wt.%)	MnO (wt.%)	MgO (wt.%)	CaO (wt.%)	Ce an S.N	Pr an. S.N	Eu an. SN	#	δ^{56}Fe	1 s	δ^{57}Fe	1 s	Mineralogy	Sample Description
A6 Drill Core, MN																	
A6-1344'	SIF	17.22	1.12	49.77	4.11	3.02	2.46	0.77	1.01	1.64	2	0.51	0.08	0.74	0.16	Magnetite, Ankerite, Siderite, Chert	Finely-laminated iron formation
Cliffs Erie Mine																	
2WX-3	HRS		0.03	1.89	0.07	0.16	0.01	0.74	1.06	1.12	8	0.04	0.09	0.06	0.13	Chert, Hematite, minor Magnetite, Siderite, Ankerite	Flat laminated stromatolite
2WX-4	HRS		0.03	8.39	0.57	0.68	1.12	1.14	0.84	1.30						Chert, Magnetite, Hematite	Small hemispheroidal stromatolite
2WX-5	HRS	91.90	0.05	6.75	0.17	0.05	0.08	1.04	0.89	1.48	6	0.45	0.03	0.67	0.05	Chert, Hematite	Small hemispheroidal stromatolite
AB-3	HRS	91.80	0.08	5.82	0.49	0.03	0.05	0.68	1.02	1.79	2	−0.02	0.04	−0.06	0.06	Chert, Hematite	Small columnar stromatolite
AB5	HRS	87.55	0.08	11.61	0.02	0.04	0.07	0.96	0.94	1.47	2	0.41	0.05	0.61	0.07	Chert, Hematite, Magnetite	Small hemispheroidal stromatolite
AB5-2	HRS		0.08	8.12	0.02	0.04	0.06	1.08	0.87	1.43	4	0.35	0.00	0.56	0.01	Chert, Hematite, Magnetite	Small hemispheroidal stromatolite
AB-9	CIF	49.18	0.86	38.74	0.03	2.40	4.40	0.76	1.03	1.15	2	0.80	0.07	1.15	0.10	Chert, Hematite, Siderite, Ankerite	Laminated iron formation
AB-17	HRS		0.09	8.47	0.02	0.04	0.06	1.10	0.89	1.41	4	0.45	0.02	0.63	0.05	Chert, Hematite	Small columnar stromatolite
AB-21	HRS		nd	nd	nd	nd	nd	0.70	1.06	1.63						Chert, Hematite	Small columnar stromatolite
LA-LS-1	SIF	34.01	0.65	41.40	1.01	3.55	0.48	1.03	0.89	1.57	2	0.49	0.08	0.67	0.11	Chert, Ankerite, Siderite, Hematite, Magnetite, Stilpnomelane, minor Pyrite	Laminated iron formation
Devils Icebox Mine																	
AB11	SIF		0.27	39.05	0.08	0.05	0.08	0.94	0.96	1.43	4	0.38	0.06	0.56	0.09	Chert, Hematite, Magnetite,	Finely-laminated iron formation
DI3	SIF		0.36	37.00	0.08	0.13	0.04	0.93	0.93	1.42						Chert, Hematite, Magnetite,	Finely-laminated iron formation
Empire Mine																	
AB4	SIF		0.72	49.43	0.27	0.57	0.52	0.81	0.99	1.46	3	0.62	0.14	0.94	0.18	Magnetite, Hematite, detrital Quartz, Chert	Finely-laminated iron formation with Grypania fossils
Eveleth Mine																	
DE-ONC-1	MnRM	68.76	0.09	15.15	5.30	0.60	1.12	0.53	1.23	1.49						Chert, Hematite, Magnetite, Pyrolusite, Siderite	Several >3 cm in diameter spheroidal oncoids
DE-ONC-2	MnRM		0.12	9.75	3.20	0.25	0.34	0.44	1.28	1.64						Chert, Hematite, Magnetite, Pyrolusite	5 cm in diameter elongated oncoid
DES-1	HRS		0.03	3.77	0.03	0.51	0.06	0.91	1.02	1.40	4	0.07	0.02	0.14	0.03	Chert, Hematite, minor Magnetite	Small columnar stromatolite
DES-2	HRS		0.03	1.67	0.02	0.04	0.03	0.82	0.99	1.41						Chert, Hematite	Small columnar stromatolite
DES-3	HRS		0.11	6.87	0.36	0.24	0.17	0.98	0.95	1.22						Chert, Hematite, minor Magnetite	Small columnar stromatolite
EM-Mn-1	MnRM	65.69	0.09	14.83	2.23	13.05	0.17	0.53	1.14	1.43	3	−0.29	0.01	−0.44	0.05	Chert, Magnetite, Hematite, Pyrolusite	6 cm long ovoid oncolite
GF-3 Drill Core																	
DH3-27	CIF		0.23	29.32	0.41	0.41	16.00	1.19	0.88	1.78	3	0.64	0.05	1.01	0.06	Magnetite, Hematite, Dolomite, Siderite, Ankerite, Chert	Alternating Fe oxide-rich and carbonate-rich bands
DH3-42	SIF		11.25	25.95	0.03	2.86	0.23	1.07	0.98	1.43						Hematite, Magnetite, Chert, Siliciclastics	Finely-laminated iron formation
DH3-43	SIF		7.93	31.13	0.03	2.69	0.66	1.11	0.94	1.36						Hematite, Chert	Finely-laminated iron formation
Kakabeka Falls																	
AB-KF-1	SIF		0.25	36.51	1.98	3.97	10.43	0.80	1.02	1.38	2	0.67	0.08	0.96	0.12	Chert, Siderite, Ankerite, Magnetite, Greenalite	Finely-laminated iron formation
GF-IF-1	HRS		0.32	1.62	0.03	0.16	0.34	1.14	0.86	1.72	2	0.62	0.01	0.86	0.01	Chert, Hematite, minor Carbonate phase	Conical columnar stromatolite
GF-IF-10																	
GF-KF-2	MRS		0.31	3.53	0.08	0.24	0.10	0.90	1.05	1.33	6	0.65	0.06	0.96	0.10	Chert, Hematite	Conical columnar stromatolite
GFM-12	MRS		0.32	2.21	0.16	0.15	0.98	1.17	0.90	1.74	6	0.52	0.04	0.75	0.05	Chert, Hematite	Columnar stromatolite

LWD-99-2 Drill Core																	
317-4			0.30	8.60	0.13	0.76	0.27				3	−0.29	0.12	−0.35	0.18	Chert, Siderite	Clast-free section of granular chert
317-6	CIF		0.00	0.79	0.01	0.01	1.43	0.81	1.21						1.21	Chert, minor Siderite or Greenalite	Granular chert
317-8	CIF		1.04	40.70	2.45	4.54	8.06	1.17	0.90	1.39	4	0.15	0.04	0.25	0.04	Chert, Siderite, Ankerite	Clast-free section of granular chert
317-10	CIF	9.11	1.19	79.44	0.99	1.65	0.80	1.13	0.88	1.39	2	0.54	0.11	0.82	0.08	Magnetite, Hematite, Chert	Clast-free section of thinly bedded chert
317-12	CIF	11.41	1.65	74.03	1.08	2.36	1.69	1.24	0.87	1.56	4	−0.35	0.03	−0.54	0.04	Siderite, Ankerite, Chert	Clast-free section of granular chert
317-13	MnRM	47.84	0.10	20.17	10.07	2.29	3.48				4	−0.66	0.09	−0.93	0.09	Chert, Hematite, Pyrolusite, Ankerite	Columnar stromatolite accreting from oncoids and rounded clasts
LWD-99-2 Drill Core																	
317-19	CIF		0.00	0.48	0.01	0.00	0.00	0.85	1.00	1.24						Chert, Magnetite	Granular chert
317-20	CIF		0.10	3.04	0.39	0.21	0.17	0.87	1.02	1.37						Chert, Magnetite, Siderite, minor Pyrite	Thinly-bedded chert
317-22	SIF		0.07	27.48	1.68	3.25	2.71	0.82	0.98	2.46	2	0.80	0.07	1.15	0.10	Chert, Magnetite, Siderite, Ankerite	Bedded chert
317-26	SIF		1.08	39.39	2.23	4.09	7.05	1.16	0.90	1.35						Chert, Hematite, minor Greenalite and Pyrite	Bedded chert
Mink Mountain																	
MM-1	HRS		0.04	3.12	0.24	0.09	0.02	0.85	0.94	1.78	3	−0.22	0.09	−0.34	0.06	Chert, Hematite, minor Siderite	Small columnar stromatolite
MM2	HRS		0.03	1.17	0.02	0.02	0.02	1.26	0.81	1.42	3	0.07	0.02	0.16	0.07	Chert, Hematite	Flat-laminated stromatolite
MM2(A)	HRS		0.20	11.44	0.14	0.23	0.05	1.26	0.81	1.40						Chert, Hematite	Oncoids-associated with MM2
MM3	HRS		0.04	1.54	0.02	0.01	0.01	1.10	0.87	1.53						Chert, Hematite, Magnetite	Small columnar stromatolite
MM4	HRS		0.01	0.21	0.00	0.00	0.00	1.28	0.80	1.37						Chert, Hematite	Small columnar stromatolite
Norway, MI																	
Curry1	CIF	0.31	29.18	0.00	0.34	0.03	0.88	0.96	1.34	3	0.40	0.05	0.57	0.07		Chert, Magnetite	Massive coarse-grained iron formation
Curry2	CIF	38.42	0.67	59.53	0.00	0.53	0.03	0.82	1.01	1.34	3	0.40	0.05	0.63	0.09	Magnetite, Chert	Massive coarse-grained iron formation
Schreiber Beach																	
GFM-1	MRS	94.28	0.33	1.17	0.02	0.04	1.19	0.89	0.99	2.14	6	0.67	0.02	0.99	0.02	Chert, Hematite	Columnar stromatolite
GFM-2-Si	MRS		0.08	0.22	0.05	0.03	0.07	0.91	0.96	1.83	2	0.37	0.02	0.52	0.00	Chert, minor Hematite	Iron-poor chert from columnar stromatolites
GFM-3	MRS		3.13	6.04	0.03	1.25	0.98	1.16	0.93	2.06	4	0.22	0.03	0.36	0.05	Chert, Hematite, minor Carbonate phase	Columnar stromatolite
GFM-5	MRS		0.20	1.33	0.03	0.02	1.33	0.82	1.03	2.15	3	0.70	0.03	1.03	0.05	Chert, Hematite, minor Carbonate phase	Flat-laminated stromatolite
GFM5-2	MRS		0.54	1.80	0.03	0.16	0.93	0.85	1.01	2.21	3	0.49	0.02	0.72	0.02	Chert, Hematite	Columnar stromatolite
GFM-7	MRS		99.15	0.12	0.23	0.00	0.01	0.16	1.03	0.94	2.57					Chert, Hematite	Iron-poor chert from columnar stromatolites
GFM8-2	MRS	0.10	0.54	0.05	0.05	0.13	0.99	0.96	2.25	2	0.52	0.01	0.82	0.03		Chert, Hematite	Columnar stromatolite
GFM-11	MRS	94.71	0.06	1.90	0.08	0.05	0.06	0.75	1.03	2.01	3	0.53	0.02	0.80	0.04	Chert, Hematite	Flat-laminated stromatolite
GFM14	MRS	0.04	0.38	0.03	0.01	0.02	0.83	1.02	1.86	6	0.82	0.04	1.25	0.04		Chert, minor Hematite	Iron-poor chert from columnar stromatolites

Facies types are: CIF — cherty iron formation, HRS — hematite-rich stromatolite, MRS microfossil-rich stromatolite, MnRM — Mn-rich microbialite, SIF — slaty iron formation. Ce–Pr–Eu anomalies are shown relative to post-Archean Australian shale (PAAS). The number symbol indicates duplicate analysis for iron isotope composition.

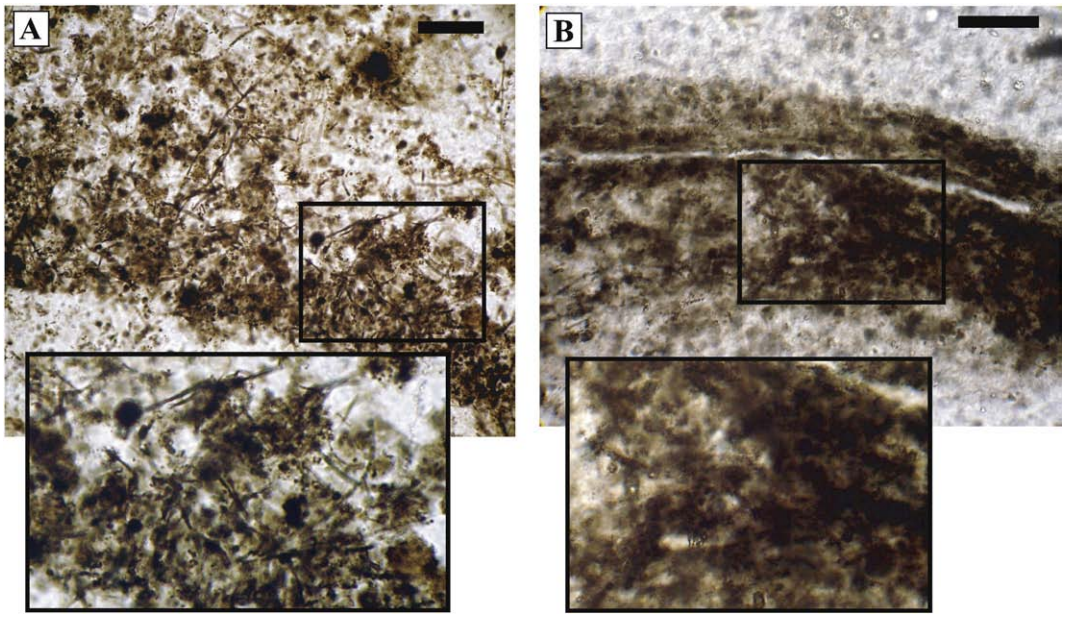

Fig. 2. Stromatolite microstructure. (A) Microstructure of the microfossil-rich stromatolites, which have microbial filaments associated with iron oxides. (B) Microstructure of the hematite-rich stromatolites, where laminae are defined by varying amounts of iron oxides. Photos are in plane-polarized light. Scale bar is 50μm.

stromatolites in the Gunflint Iron Formation contain cubic pyrite and are often organic-rich and lack iron oxides. These and the carbonate stromatolites were not investigated in this study.

Iron-bearing siliceous columnar and flat-laminated stromatolites are found in two laterally correlative units in both the Gunflint and Biwabik Iron Formations. The stromatolites are associated with thinly laminated and granular iron-formations and occasionally with hummocky cross-stratified grainstones, suggesting subtidal deposition above the storm wave base. There is a gradation from laminae composed of microfossils, diffuse organic matter, and iron oxides (Fig. 2A) to colloidal or densely-packed iron-rich laminations with low organic carbon content (Fig. 2B). Presence of this gradation on a small scale likely reflects control of original composition (e.g. relative levels of Fe- and Si-enrichments) on early diagenetic alteration and taphonomy. Horizons with extensive early silica precipitation would have had a better potential to preserve microfossils and protect iron oxides from later remineralization and recrystallization. Despite the presence of a continuum in microstructures and stromatolite morphologies, we distinguish between the microfossil-rich stromatolites and those with more distinct laminae defined by bands of iron oxides. The stromatolites that generally lack microfossils are herein referred to as hematite-rich stromatolites, based on their main primary non-siliceous mineralogical component.

The most abundant microfossil, *Gunflintia*, is characterized by randomly oriented filaments commonly coated by iron oxides. These features are characteristic of the modern iron bacterium *Leptothrix* (Knoll and Simonson, 1981; Strother and Tobin, 1987). Although some of the Gunflint biota appear to be planktonic, including coccoidal forms, the dense intertwined filaments of *Gunflintia* appear to represent a preserved benthic microbial ecosystem (Hofmann, 1969; Strother and Tobin, 1987). *Gunflintia* filaments are found coating high convexity surfaces and preferentially occur in stromatolites, which provides strong evidence for a benthic lifestyle. There are rare spiral filaments that have a striking resemblance to the modern iron bacterium *Gallionella* or *Mariprofundus* (Cloud, 1965) and non-septate filaments with endospores that are similar to the iron bacterium *Crenothrix* (Barghoorn and Tyler, 1965). Columnar microfossiliferous stromatolites also contain abundant small straight and curved rods and coccoids with iron oxide-rich cell walls (Tazaki et al., 1992) that are similar to cultured aerobic iron-oxidizers (Emerson and Moyer, 1997). These features are consistent with the Gunflint biota being microaerophilic lithotrophs, but it is difficult to link simple microfossils with a specific metabolism based on morphology alone (Awramik and Barghoorn, 1977; Cloud, 1965). These microfossil morphologies have also been interpreted as cyanobacterial (Awramik and Barghoorn, 1977; Barghoorn and Tyler, 1965) and are found in ancient Fe-poor environments (e.g. Amard and Bertrand Sarfati, 1997). It is more than likely that *Gunflintia* and similarly featureless filamentous microfossils combine phylogenetically and ecologically disparate organisms. Geochemical proxies linked with paleontological observations are, therefore, needed to decipher the type of microbial metabolisms present in these ancient ecosystems.

3. Material and methods

3.1. Analytical methods

Clean rocks were crushed between two plexiglass discs inside a Teflon bag using a hydraulic press. One to five grams of rock chips from each sample without signs of secondary veins or surface weathering were selected for analyses and cleaned through several rinses with deionized water during ultrasonication. The cleaned material was powdered in an agate shatter-box and dissolved in HNO_3–HCl–HF acid mixture. Fe was purified on Bio-Rad AG1X8 anion resin and iron isotope ratios were determined with a Thermo Scientific *Neptune* multicollector inductively coupled plasma mass-spectrometer (MC-ICP-MS) following previously published methods (Rouxel et al., 2005; Rouxel et al., 2008a,b). The MC-ICPMS is operated in medium-resolution mode and we used Ni as an internal standard for mass bias correction. Fe-isotope values are reported relative to the Fe isotope standard IRMM-14 using the conventional delta notations (Table 1). Several georeference materials (Govindaraju, 1994), including one banded iron-formation (IF-G) and Hawaiian Basalt (BHVO-1) were measured. Based on duplicated chemical purification and isotope analysis the long term external reproducibility is 0.10‰ for δ^{56}Fe and 0.14‰ for δ^{57}Fe values (2 standard deviations).

Analyses of REEs + Y, Ba, were performed on a ThermoElectron Inc. Element2 ICP–MS at the Woods Hole Oceanographic Institution

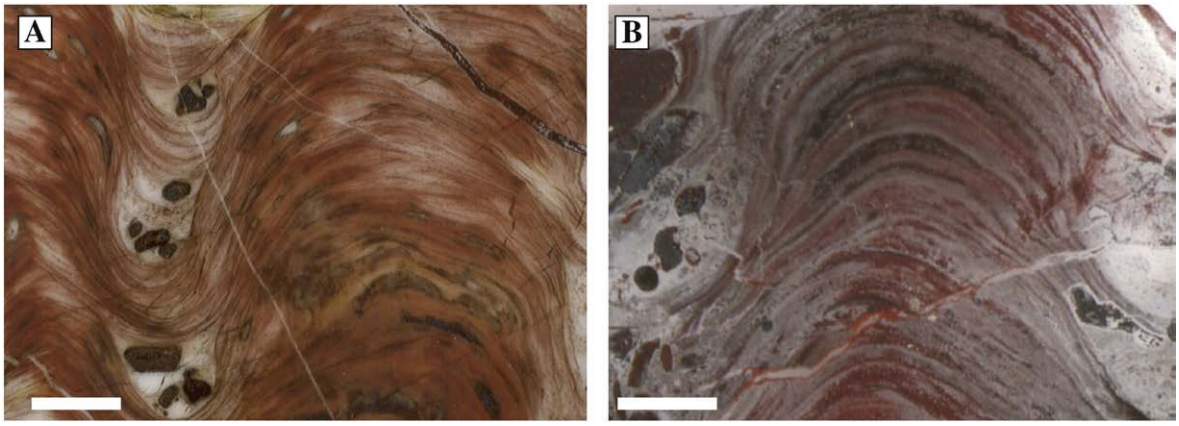

Fig. 3. Morphology of the hematite-rich stromatolites. Locally-developed red and black coloration is caused by iron oxides. (A) Laminations between columns drape over clasts and (B) Thickening of laminations at the convexity peaks indicative of microbial mediation of stromatolite formation. Photos are in reflected light. Scale bar is 1 mm.

(WHOI) and on a ThermoElectron Inc. XSeriesII at Laurentian University. At WHOI, solutions were injected into the plasma using a Cetac Aridus® desolvating nebulizer to reduce isobaric interferences (e.g., $^{135}Ba^{16}O^{+}$ on $^{151}Eu+$). Ba and REE oxide formation were monitored throughout the analytical session by periodic aspiration of Ba and Ce spikes. Ba-oxide formation was significantly less than 1%. Any isobaric interference of BaO^{+} on Eu^{+} would bias (decrease) the naturally occurring $^{151}Eu/^{153}Eu$ ratio (~0.89) measured. In almost all samples no bias was observed and no correction for BaO interference was required. REE-oxide formation was typically less than ~4% of total REE concentration. Samples were spiked with 5 ppb In internal standards to correct for fluctuations of the plasma during the analytical session. Unknown sample concentrations were calibrated against matrix-matched, multi-REE standards prepared from Specpure plasma solution standards. Background intensities were measured periodically by aspirating 5% HNO_3 blank solution. Based on multiple analyses of selected samples across multiple analytical sessions, the accuracy of our analyses is conservatively estimated to be ±10% and rare earth element ratios are estimated to be accurate within ±5%. Analytical precision and the accuracy for our measurements of REE abundances and ratios were also checked by multiple analyses of the geostandards IF-G and BHVO-1. At Laurentian University, trace element concentrations were analyzed using a method modified after Eggins et al. (1997) that employs both

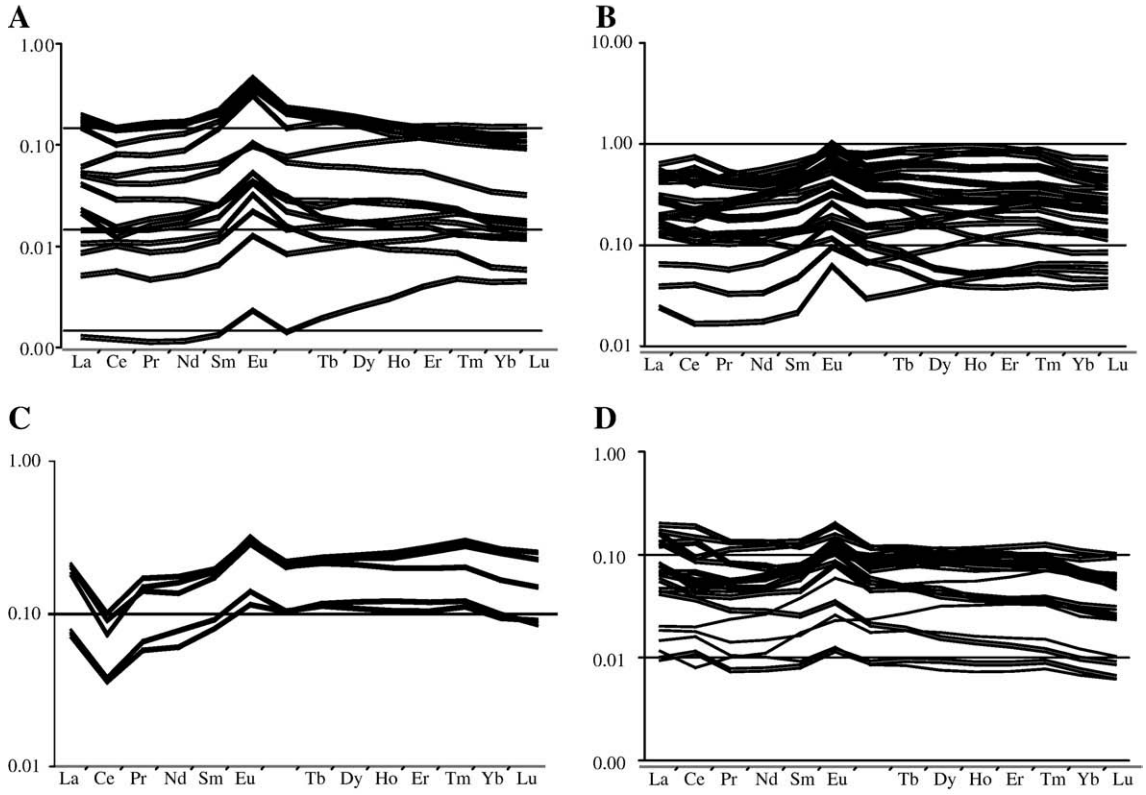

Fig. 4. Rare earth element patterns for the components of the iron formations normalized to post-Archean Australian shale (PAAS): (A) Microfossil-rich stromatolites; (B) Cherty and slaty iron formations; (C) Mn-rich oncoids; and (D) Hematite-rich stromatolites. Gd data are not reported and the REE patterns are plotted with Gd having linearly extrapolated from Dy and Ho data.

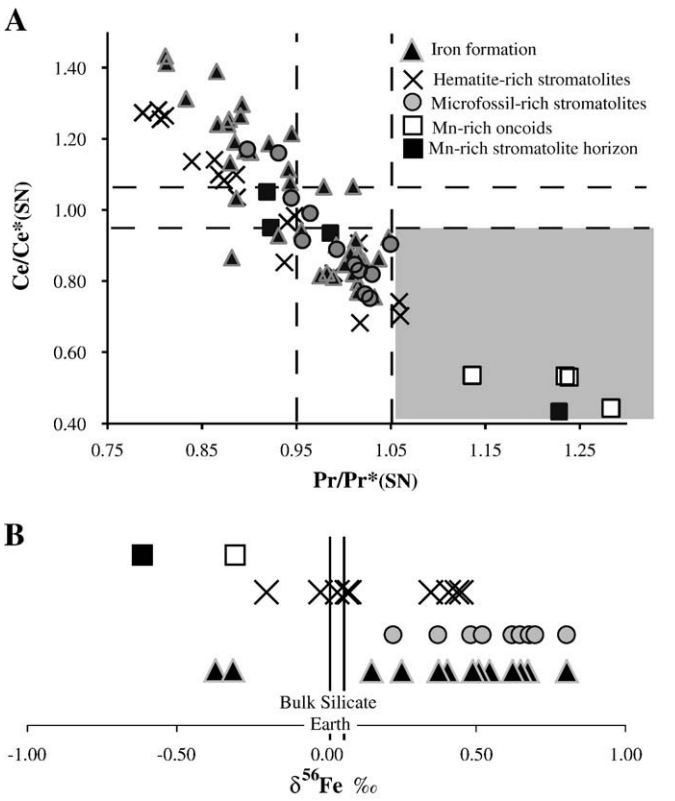

Fig. 5. Geochemical results for components of the iron formations. (A) Ce anomaly normalized to post-Archean Australian shale (PAAS). The true Ce anomaly is displayed by the grey area that corresponds to values of the Ce/Ce* (Ce/(0.5Pr + 0.5La) and the Pr/Pr* (Pr/(0.5Ce + 0.5Nd)) above and below the unity, respectively. This approach described in Bau and Dulski (1996) discriminates between positive La and true negative Ce anomalies. (B) Iron isotope composition of stromatolites and iron formations normalized to the international standard IRMM-14 and defined as $\delta^{56}Fe = 1000^{*}$ $(^{56}Fe/^{54}Fe_{sample}/^{56}Fe/^{54}Fe_{IRMM14} - 1)$. The Fe isotope value of the bulk silicate Earth is close to 0.09‰ while $\delta^{56}Fe$ values of seawater influenced by hydrothermal and diagenetic Fe fluxes is likely below −0.3‰ (Anbar and Rouxel, 2007). Positive $\delta^{56}Fe$ values in stromatolites and iron formations indicate partial Fe(II) oxidation in O_2-depleted environments.

internal standards (^{6}Li, In, Re, Bi and ^{235}U) as well as external drift correction. The instrument was tuned to 1.5% CeO^{+}/Ce^{+} and all isobaric interferences were corrected for using oxide formation rates determined from pure elemental solution measured immediately after the samples. With this method, REE in basaltic rock standards such as BHVO-1 and -2, can be reproduced to better than 1% rsd (see Kamber, 2009, for more information) using a quartz spray chamber.

Major elements in the iron formations (Fe, Al, Ca, and Mg) were also determined using the medium-resolution mode of the *Element II* at WHOI with a quartz spray chamber. Similar to the REE procedure, In was used as an internal standard and the data were calibrated by standardization to the geostandard BHVO-1. Analytical precision and accuracy of element abundances were again checked by multiple analyses of the geostandards IF-G and BHVO-2 and reproducibility was better than 5%. Selected samples representative of the various matrices were sent to Activation Laboratories Ltd. (Ancaster, Ontario) for additional geochemical analysis. Major and trace elements were analyzed at Activation Laboratories by ICP-AES and ICP-MS, respectively, after lithium metaborate/tetraborate fusion. Major element compositions and REE patterns determined by both techniques were within 7%. Mineralogy was determined through a combination of standard petrographic techniques and X-Ray diffraction (XRD) using a PANalytical X'pert Pro diffractometer.

4. Results

4.1. Geochemistry of the Animikie basin stromatolites and iron formations

Samples of iron formation and stromatolites consist mainly of silica and iron. Iron concentrations in the iron formation samples vary from 0.5% to 66.5% Fe_2O_3, while Fe concentrations in microfossil-rich and hematite-rich stromatolites vary from 0.5% to 10.8% Fe_2O_3 (Table 1). Mn concentrations in the iron formations and siliceous stromatolites are typically low (<0.1% MnO). However, there is a 1 to 3 meter thick shallow-water horizon located in the Upper Cherty Member of the Biwabik Iron Formation with abundant siliceous oncoids and stromatolites that is strongly enriched in manganese oxides (Zielinski et al., 1994). Some slaty and granular iron formation samples also display Mn-enrichments (Table 1); however, these enrichments do not show a clear stratigraphic trend. Oncoids and other Mn-enriched microbialite samples contain between 2.2% and 9.64% MnO. All samples contain less than 0.15% sulfur. Most of the analyzed samples contain low amounts of Al, Ti, and Ga, which is consistent with a small contribution of detrital siliciclastic material (Table 1 and Appendices 2 and 3 for additional data).

The shale-normalized (post-Archean Australian shale—PAAS; Nance and Taylor, 1976) REE patterns are shown in Fig. 4. REE abundances range from ~0.001 to 0.5 those of PAAS. Positive Eu anomalies are present in most analyzed samples (Fig 4). The shallow-water Mn-rich oncoids display light REE depletion and strongly negative Ce anomalies. The siliceous stromatolites and iron

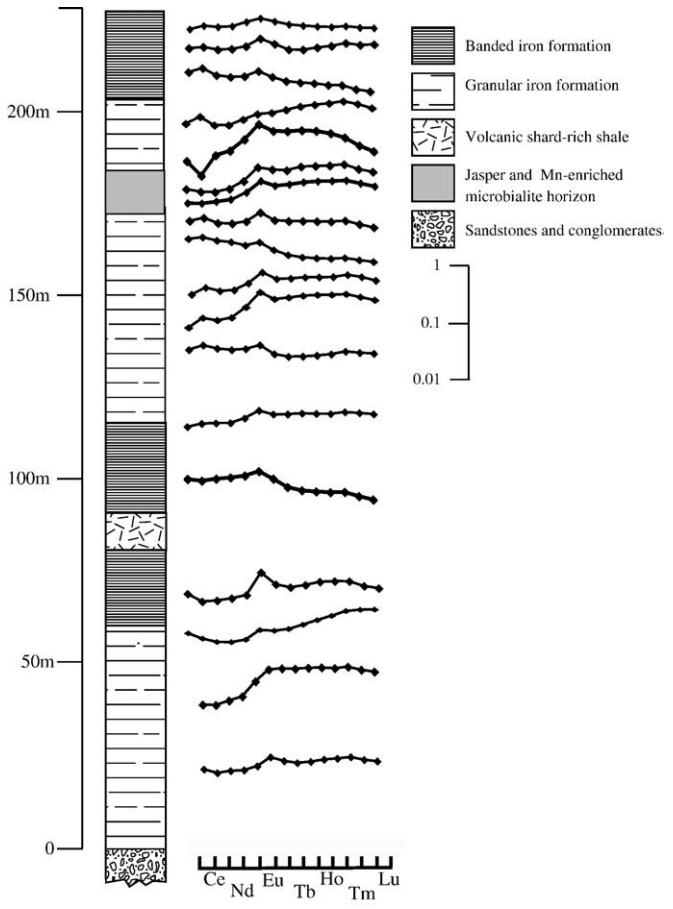

Fig. 6. Post-Archean PAAS-normalized REE patterns for samples from the LWD-99-2 drill core through the Biwabik Iron Formation. Note large variations in the light/heavy REE ratios without any systematic stratigraphic trend.

formations, in contrast, lack significant negative Ce anomalies. There are both negative and positive Ce anomalies in samples from the horizon of siliceous Mn oxide-enriched columnar stromatolites (Fig 5A). True negative Ce anomalies, as presented in Fig 5A, have $Ce/Ce^*(Ce/(0.5Pr+0.5La)$ and $Pr/Pr^*(Pr/(0.5Ce+0.5Nd))$ values above and below the unity, respectively. This approach discriminates between positive La and true negative Ce anomalies (Bau and Dulski, 1996).

There is a range from light REE depletion to light REE enrichment in the shale-normalized REE patterns in both stromatolites and samples of iron formation. There is no systematic stratigraphic shift in light to heavy REE ratios in the LWD-99-2 drill core (Fig. 6), which goes through the entire Biwabik Iron Formation. Gradual basin isolation, potentially related to large-scale tectonic processes (cf. Kamber et al., 2004) is, therefore, an unlikely control over the observed variability in the light to heavy REE ratios. Light to heavy REE ratios do not co-vary with the amount of siliciclastic contribution (e.g. there is no co-variation on a Pr/Yb vs. Al_2O_3 cross-plot).

Iron isotope data for various lithotypes of the Animikie basin iron formations are shown in Fig 5B and reported in Table 1. The Gunflint microfossiliferous stromatolites contain exclusively positive $\delta^{56}Fe$ values that range from +0.22 to +0.82‰. The microbialites lacking microfossils (hematite-rich stromatolites and Mn-rich microbialites) generally yield lower $\delta^{56}Fe$ values than the microfossiliferous stromatolites with values ranging from −0.66 to +0.45‰. There is a negative correlation between Mn/Fe ratios and $\delta^{56}Fe$ values in the microbialites lacking microfossils (hematite-rich stromatolites and Mn-rich microbialites), with the most Mn enriched samples containing the lowest $\delta^{56}Fe$ values (Fig. 7). Samples of granular and banded iron-formations have $\delta^{56}Fe$ values ranging from −0.35 to +0.81‰, but predominantly contain positive values. There is no significant correlation between $\delta^{56}Fe$ values and Mn/Fe ratios in samples of iron formation or microfossil-rich stromatolite (Fig. 7).

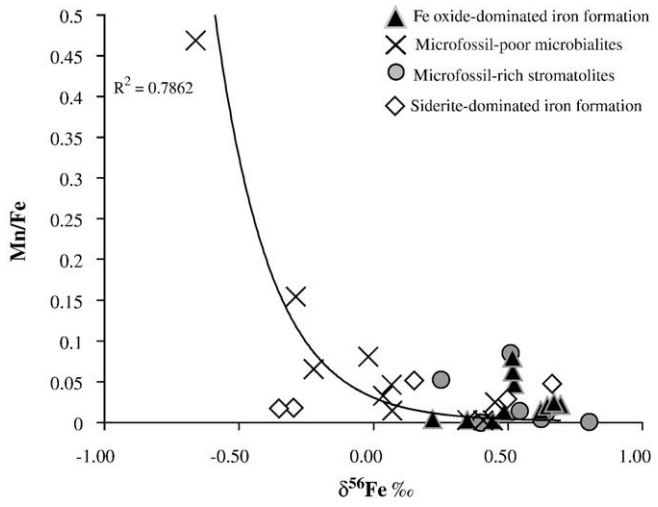

Fig. 7. Crossplot of Mn/Fe ratios and $\delta^{56}Fe$ values for components of the iron formations. There is an exponential relationship ($y=0.0297e^{-4.826x}$) between Mn/Fe ratios and $\delta^{56}Fe$ values for the microfossil-poor microbialites (hematite-rich stromatolites and Mn-rich stromatolites and oncoids). The solid black line shows the trend for this subset of samples. This correlation might suggest that the low $\delta^{56}Fe$ values reflect periods of quantitative Fe-oxidation. Fe-oxidation occurs at lower redox potential than Mn-oxidation and, therefore, under conditions of Mn-oxidation, quantitative Fe oxidation will take place resulting in precipitation of iron oxides recording seawater values, which are likely to be negative. An exponential relationship between Fe isotope values and Mn/Fe ratios should be expected since iron oxidation generally follows a Rayleigh-type fractionation. There is no significant correlation between Mn/Fe ratios and $\delta^{56}Fe$ values for the samples of iron formation or microfossil-rich stromatolites.

5. Discussion

5.1. REE systematics and basin-scale redox structure

Since microbial iron-oxidation at or near neutral pH occurs in low oxygen (i.e. microaerophilic) conditions, linking the preserved microbial community with dysoxia is an essential aspect of demonstrating the presence of an iron-oxidizing microbial ecosystem. REE systematics can be used as a tool to constrain redox conditions in the overlying water column. In general, there are strong water-column negative cerium (Ce) anomalies when normalized to shale composites in oxygenated marine settings while suboxic and anoxic waters lack significant negative shale-normalized dissolved Ce anomalies (Byrne and Sholkovitz, 1996; German and Elderfield, 1990). Oxidation of Ce (III) greatly reduces Ce solubility resulting in preferential removal onto reactive surfaces, such as Mn–Fe oxyhydroxides, organics, and clay particles (Byrne and Sholkovitz, 1996). In suboxic and anoxic waters, Ce anomalies are slightly negative, absent, or positive due to reductive dissolution of Ce(IV) and settling Mn–Fe-rich particles that carry positive Ce anomaly with respect to the seawater (Byrne and Sholkovitz, 1996; German et al., 1991). Similarly, light REE depletion develops in oxidized water bodies due to preferential removal of light versus heavy REEs onto Mn–Fe oxide particles, organic matter, and clay particles and the ratio of light to heavy REEs markedly increases across redox-boundaries due to reductive dissolution (Byrne and Sholkovitz, 1996; German et al., 1991).

The REE patterns of siliciclastic-free Fe-rich sediments (e.g. cherts, jasper) can be used as a qualitative paleoseawater redox proxy (Bau, 1999; Bau and Dulski, 1996; Slack et al., 2007). Based on experimental results, there is negligible amounts of oxidative scavenging of Ce on Fe oxyhydroxide surfaces, unlike Mn oxides, at pH conditions >5 relevant to marine environments (Bau, 1999; Ohta and Kawabe, 2001). Therefore, iron oxides qualitatively record Ce anomalies from the water column from which they precipitated, while Mn oxides will be influenced by preferential Ce scavenging. REEs in siliceous iron oxide-rich sediments appear to be rock buffered under low water–rock ratios typical of most early to late stage diagenetic and metamorphic alteration conditions (Bau, 1993). Therefore, REEs in iron formations have utility as paleoredox proxies.

Well-established facies and sequence stratigraphic framework for deposition of iron formations in the Animikie Basin (Ojakangas, 1983; Ojakangas et al., 2001) allows us to place the REE data into a bathymetric context. The shift from positive or nonexistent to strongly negative Ce anomalies from deeper-water banded iron formations to the tidal zone in the Gunflint and Biwabik iron formations indicates the presence of a strong redoxcline. The lack of negative Ce anomalies in the microfossiliferous and hematite-rich stromatolites (Fig. 4A) suggests that stromatolites formed in low oxygen environments below or at the redoxcline, the ideal conditions for lithotrophic ecosystems. Essentially pure chert sections of the stromatolites similarly lack negative Ce anomalies (Table 1) further supporting that bulk stromatolite samples qualitatively reflect ambient seawater composition and that the lack of negative Ce anomalies is not an artifact of Ce scavenging by metal oxides. The presence of excess amounts of Eu, even in shallow-water depositional environments, is consistent with widespread anoxia and a strong high temperature hydrothermal metal flux into the shallow Animikie sea from the deep ocean (Kamber and Webb, 2001). Consequently, Fe–Mn nodules and crusts in the deep ocean were not significant Ce sinks in the late Paleoproterozoic ocean Ce cycle.

The presence of strongly negative Ce anomalies in manganese-rich oncoids that formed in the tidally-influenced zone under shallower conditions than the subtidal stromatolites (Awramik and Barghoorn, 1977; Cloud, 1965; Zielinski et al., 1994), indicates strongly oxidizing conditions in nearshore environments. There must have been limited Ce oxidation and sorption onto the oncoid Mn oxides in order for them

to record negative anomalies, similar to some distal hydrothermal Mn–Fe rich sediments formed in oxic conditions (e.g. Barrett and Jarvis, 1988). Positive and negative Ce anomalies in the horizon of Mn-enriched columnar stromatolites reflect either stromatolite growth under changing redox conditions or varying levels of Ce scavenging on Mn oxides. Strong negative Ce anomalies in the shallow waters – in the absence of a significant Ce sink on slowly forming Mn nodules and crusts in the deep ocean – can be assumed to be due to scavenging of Ce(IV) on organic-Mn–Fe-rich clay particles in shallow-waters and estuaries.

Variability in light to heavy REE ratios in stromatolites and samples of iron formation might similarly reflect formation below or at a redoxcline. The lack of a stratigraphic trend in REE patterns rules out the possibility of light REE-enrichment linked with a light REE-enriched terrestrial flux that could be expressed in the water column due to basin isolation. The lack of significant co-variation between light and heavy REE ratios and detrital element concentrations rules out the possibility that the level of siliciclastic input is the predominant control over the trivalent REE patterns.

Redox dependant Mn cycling in the suboxic zone can dramatically alter REE patterns by decreasing the level of light REE depletion (e.g. German and Elderfield, 1990). We interpret the large range of light to heavy REE ratios in the Animikie iron formations as an indication of stromatolite accretion and iron formation deposition in water masses with varying contribution of REE from Mn-oxide dissolution. This interpretation implies suboxic deposition and iron precipitation mediated by iron-oxidizing bacteria for samples with light REE enrichment. The presence of light REE depletion in shallow-water environments is consistent with REE ocean cycle influenced by a Mn-oxide shuttle from shallow-water oxidized setting to deeper-water environments.

5.2. Iron isotopes as tracers of redox dynamics

The distribution of iron within the stromatolites suggests direct microbially-mediated iron precipitation. Iron in the microfossiliferous stromatolites is predominately associated with the microfossil-rich laminae. The hematite-rich stromatolites also contain Fe-oxides within isolated laminae (Brotton et al., 2007), which have been observed to thicken at their apices and drape over intercolumnar clasts rather than radiating from or infilling space around them (Fig. 3AB). These features are difficult to explain through direct abiotic precipitation from seawater and indicate that iron enrichment, and associated Fe-isotope composition, can be directly linked to benthic microbial mats.

The disparate redox properties of cyanobacterial and iron-oxidizing microbial mats are likely to be reflected in bulk sample iron isotope values, offering a means to distinguish between these microbial communities. In modern cyanobacteria dominated microbial mats, oxygen commonly has over a fivefold higher concentration than the ambient level (Jorgensen et al., 1983). As a consequence, ferrous iron is quantitatively oxidized even in thin, modern cyanobacterial microbial mats growing in the presence of ferrous iron concentrations greater than 100 μM (Trouwborst et al., 2007). This concentration is twice the estimate of dissolved ferrous iron in anoxic Archean and Paleoproterozoic oceans (Holland, 1984). Iron oxides precipitated in fully oxygenated conditions are expected to have the same δ^{56}Fe values as the dissolved iron sources because of near complete iron oxidation and precipitation. In contrast, partial ferrous iron oxidation, which is expected in iron-oxidizing microbial mats, produces iron oxides with positive δ^{56}Fe values relative to the Fe(II) source. Accordingly, modern ferric Fe-oxides from open-marine sediments (e.g. hydrous ferromanganese oxides) have negative δ^{56}Fe values between 0 and −1‰ (Beard et al., 2003; Johnson and Beard, 2006; Levasseur et al., 2004; Zhu et al., 2000), reflecting, presumably, the Fe-isotope composition of seawater. Variably negative δ^{56}Fe values may reflect the contribution of various oceanic Fe sources, such as atmospheric input, sediment porewaters, riverine and groundwater inputs, and hydrothermal sources (Anbar and Rouxel, 2007; Chu et al., 2006; Rouxel et al., 2008b; Severmann et al., 2004b; Staubwasser et al., 2006). Cyanobacterial mats turn anoxic in light limiting conditions, but also appear to be characterized by negative δ^{56}Fe values (e.g. (Severmann et al., 2004b). Additionally, in Fe-rich cyanobacterial mats, pore water Fe concentrations during anoxic conditions (i.e. night time) are lower or equivalent to those in the overlying water (e.g. Trouwborst et al., 2007), suggesting minimal secondary iron loss.

In contrast, ferric Fe-oxides formed in oxygen-depleted environments, either by slow abiotic Fe-oxidation or bacterial Fe-oxidation, can be expected to have near zero or positive δ^{56}Fe values (Balci et al., 2006; Croal et al., 2004; Dauphas et al., 2004; Rouxel et al., 2005; Rouxel et al., 2007). The exclusively positive δ^{56}Fe values from iron oxides in the microfossiliferous stromatolites (Fig 5B), therefore, indicate that there was partial Fe(II) oxidation within dense microbial mats. The lack of quantitative oxidation is at odds with an oxygenic photosynthetic microbial community mediating iron oxidation and precipitation.

Iron isotope fractionation during abiotic or biogenic iron oxidation at near-neutral pH generally follows a Rayleigh distillation process and can, therefore, be used to estimate the fraction of the ferrous iron load that was oxidized assuming closed system conditions (Balci et al., 2006; Bullen et al., 2001; Croal et al., 2004). The mean iron isotope composition of the precipitating Fe-oxide reservoir (δ^{56}Fe(III)$_{ppt}$) can be described by the following equation:

$$\delta^{56}Fe(\mathrm{III})_{ppt} = \delta^{56}Fe(\mathrm{II})_i + \varepsilon \ln(f) f / (1-f),$$

where δ^{56}Fe(II)$_i$ is the initial isotopic composition of the Fe(II)$_{aq}$; epsilon (ε) is the isotopic fractionation factor during oxidative Fe(III) precipitation; and f is the fraction of Fe(II)$_{aq}$ remaining in solution. Assuming that the dissolved ferrous iron source from which the ecosystems forming the microfossil-rich stromatolites precipitated ferric oxides had δ^{56}Fe values at or lower than −0.5‰ and ε factor between 1.0 and 1.5‰ (Balci et al., 2006; Bullen et al., 2001; Croal et al., 2004), the δ^{56}Fe values for Fe-oxides in microfossiliferous stromatolites between 0.82‰ and 0.22‰ correspond to oxidation of ~30% to~65% of the ferrous iron load at the site where stromatolites formed.

It is generally accepted that in a redox stratified ocean forming banded iron formations, hydrothermal vent waters were the dominant source of dissolved iron (Holland, 1984). Based on δ^{56}Fe values of modern seafloor hydrothermal systems, δ^{56}Fe values of hydrothermal sources to the Animikie basin likely ranged from −0.1 to −0.9‰, with the average at around −0.3‰ (Beard et al., 2003; Rouxel et al., 2008a; Severmann et al., 2004a; Sharma et al., 2001), although precipitation of iron oxides in hydrothermal plume may further lower δ^{56}Fe value of hydrothermal dissolved iron. Diagenetic ferrous iron sources such as upwelling porewaters and groundwater with δ^{56}Fe values of <−0.5‰ (down to −5.0‰) may be also volumetrically important iron sources (Rouxel et al., 2008b; Severmann et al., 2006). Thus, it is reasonable that the dissolved iron in the shallow part of the Animikie Sea had δ^{56}Fe values at or below −0.5‰, and that using a Rayleigh fractionation model provides a suitable first-order estimate of the maximum extent of Fe (II) oxidation in benthic ecosystems forming the microfossiliferous stromatolties. Based on these results, it is difficult to reconcile the estimated levels of oxidation, i.e. around half of the Fe(II) load in the microbial mat, with a cyanobacterial interpretation for the microfossils. This interpretation assumes that there was minimal loss of isotopically light iron during early diagenesis. This is consistent with the presence of well-preserved microbial fossils coated with iron oxides (Fig. 2A), which requires exceptional preservation, since iron-encrusted microbial filaments

rapidly degrade to colloidal oxides during heterotrophic degradation (e.g. Emerson and Revsbech, 1994).

The wide range of δ^{56}Fe values in the microbialites generally lacking microfossils from −0.66‰ to 0.45‰, is likely caused by variability in the extent of iron oxidation as well as multiple Fe sources. The lowest δ^{56}Fe values may indicate that there were periods of quantitative iron oxidation in the benthic ecosystems, resulting in the preserved oxides recording negative, ambient δ^{56}Fe values. A correlation between Mn/Fe ratios and the δ^{56}Fe values in hematite-rich and Mn-enriched microbialites (Fig. 7) supports this interpretation (i.e. higher O_2 levels required to oxidize and precipitate Mn-oxides would cause quantitative Fe(II) oxidation and, therefore, negative Fe-isotope values).

Alternatively, lower δ^{56}Fe values in Fe-oxides from the stromatolites could reflect low levels of oxidation of a local isotopically light reservoir. As mentioned above, precipitation of isotopically heavy Fe-oxides before upwelling onto a shelf can produce dissolved iron with strongly negative δ^{56}Fe values (Rouxel et al., 2005) and significant benthic flux of Fe(II) from dissimilatory Fe-reduction in sediment porewaters would also produce an isotopically light reservoir (Severmann et al., 2006). Despite uncertainties about the negative δ^{56}Fe values in the hematite-rich stromatolites, the frequent occurrence of positive values indicates that limited oxidation was common in the benthic microbial ecosystems forming the stromatolites. Thus, the iron isotope data indicate that the microbial ecosystem forming the hematite-rich stromatolites induced partial Fe(II) oxidation, and strongly supports the hypothesis that the biota were a chemolithotrophic, rather than a cyanobacteria-dominated ecosystem. Again, this is consistent with some interpretations of the microfossils (Knoll, 2003; Knoll and Simonson, 1981; Strother and Tobin, 1987).

The iron formations are mineralogically more complex than the hematite-dominated microbialites, which complicates interpretation of δ^{56}Fe values. The range of δ^{56}Fe values in the iron formations likely reflect a combination of varying extent of iron oxidation, variability in the δ^{56}Fe values of ferrous iron seawater reservoir, and mineralogical control on the bulk sample δ^{56}Fe values (Dauphas et al., 2007; Johnson et al., 2003). The predominance of positive values in the iron formations suggests that partial ferrous iron oxidation was the primary depositional process for the iron formations. The only samples of iron formation with negative δ^{56}Fe values are bands of pure siderite (Fig. 7). The negative values in these samples likely reflect either the end-products of dissimilatory iron reduction or the Fe- carbonate equilibrium fractionation factors (e.g. Johnson et al., 2003).

5.3. Ecosystem reconstruction and implication for the global ecosystem evolution

Sedimentological evidence suggests the stromatolites developed in the transition zone between anoxic iron-rich deep waters and oxygenated shallow waters, likely suggesting suboxic rather than strictly anoxic or oxic conditions for deposition (Cloud, 1965). Variable Mn/Fe and light to heavy REE ratios in the siliceous stromatolites similarly suggest formation near a redoxcline, in suboxic conditions. Iron isotope data suggest a low extent of oxidation in most of the stromatolites, precluding the possibility that cyanobacteria dominated the microbial ecosystems. Thus, the geochemical and petrographic evidence presented above supports the hypothesis that lithotrophic iron oxidizers formed the Animikie basin siliceous stromatolites (Fig. 8). We recognize that the presence of strictly anoxygenic photosynthetic iron-oxidizers and nitrate-dependent iron oxidizers cannot be excluded based on Fe-isotope evidence only (Croal et al., 2004), and these metabolisms were also likely present within the examined ecosystems. However, a predominance of microaerophilic iron oxidizers is supported by microfossil evidence, which suggests the presence of iron-oxidizers, comparable to the present-day *Lepothrix, Crenothrix, Gallionella,* and *Mariprofundus* (Barghoorn and Tyler, 1965; Cloud, 1965; Golubic and Lee, 1999; Strother and Tobin, 1987).

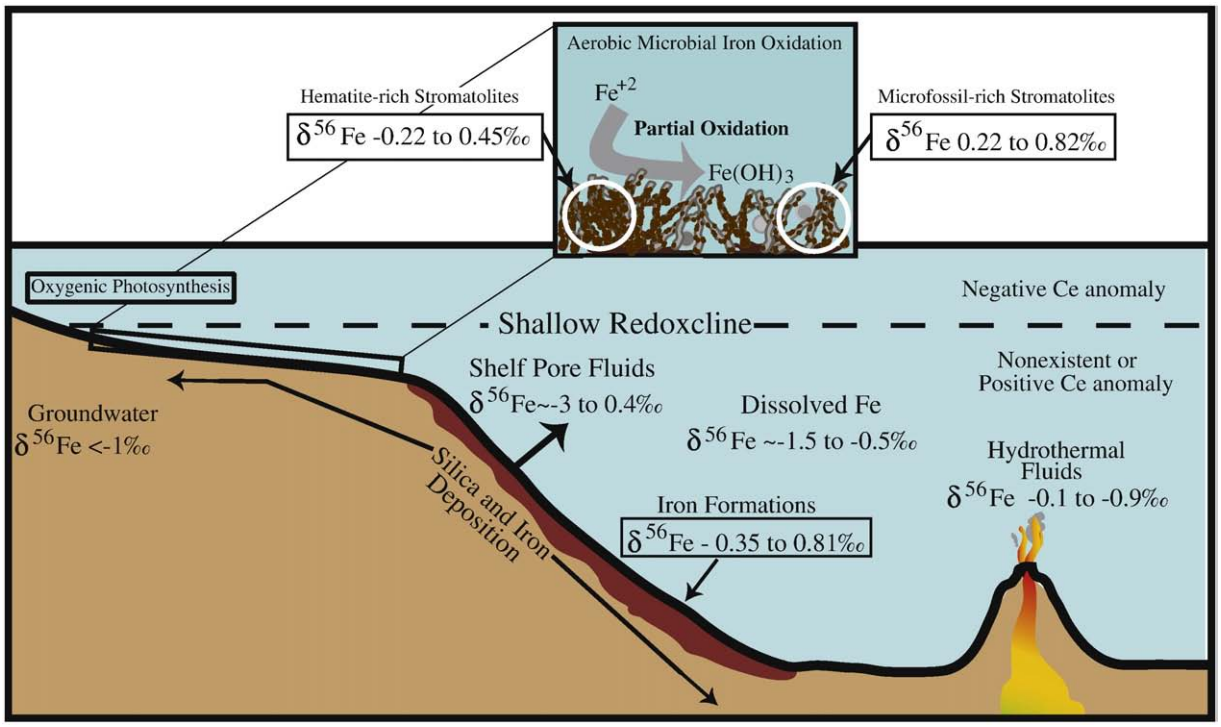

Fig. 8. Overview of the iron and REE cycles in the Animikie basin. Rare earth element patterns indicate there was formation of iron enriched stromatolites in suboxic or anoxic conditions. Fe isotopes indicate that iron formations were a sink for isotopically heavy Fe. Additionally, the dominance of positive iron isotope values in siliceous iron enriched stromatolites and iron formation indicates a partial ferrous oxidation was a common process. See text for further details.

The Animikie basin stromatolites, especially the hematite-rich stromatolites, form nearly continuous units that can be correlated for over a hundred kilometers, indicating that the chemolithotrophic microbial communities were an important shallow-marine ecosystem rather than an isolated occurrence. Evidence for strong tidal activity during deposition of the Animikie iron formations (Ojakangas et al., 2001) indicates minimal basin isolation. The iron-rich Animikie basin sedimentary system appears to be traceable from central Minnesota, USA to the Belcher Islands, Canada along the margin of the Superior craton thousands of kilometers to the northeast (Baragar and Scoates, 1981), consistent with an open ocean setting. Hematite-rich siliceous stromatolites and microfossils similar to those found in the Animikie basin are also present in the 1.88 Ga Sokoman Iron Formation in northeastern Canada (Knoll and Simonson, 1981), the ca. 1.8 Ga Chuanlinggou Iron Formation in North China (Yongding et al., 2004), the ca. 1.85 Ga Duck Creek Dolomite (Knoll and Barghoorn, 1976; Knoll et al., 1988), the ca. 1.9 Ga Dannemora Iron Formation, Sweden (Lager, 2001), and the ca. 1.85 Ga Frere Iron-Formation in Western Australia (Walter et al., 1976). It is likely, therefore, that these iron formations also preserve chemolithotrophic microbial ecosystems. However, since it is difficult to determine microbial metabolisms based on morphology alone, additional geochemical work should be done to test whether these hematite- and microfossil-rich stromatolites were indeed formed by iron oxidizers. All these iron formations, with the possible exception of poorly-dated Chuanlinggou Iron Formation of North China, are closely temporally associated with the ca. 1.89 Ga mantle plume event and contemporaneous Large Igneous Province (e.g. French et al., 2008; Halls and Heaman, 2000; Heaman et al., 1986, 2009). Although origin of this event is still debated (see Heaman et al., 2009), the following models were advanced: 1) mantle plume, 2) extension in back-arc or pull-apart settings, and 3) short-lived episode of passive astenosphere flow beneath already thinned passive margins due to abrupt change in plate boundary stress. Regardless of its origin, it was a major global event with potentially dramatic impacts on surface conditions. It is likely that the deep-ocean redox state was temporally switched to ferruginous conditions by an enhanced hydrothermal Fe flux during this event, leading to Fe-rich deep-waters upwelling onto oxidized shelves.

The apparent absence of the Gunflint-type biota or hematite-rich stromatolites in older and younger successions suggests that its appearance in the late Paleoproterozoic represents an ecosystem evolutionary event (Knoll, 2003; Knoll and Simonson, 1981; Walter et al., 1976). The late Paleoproterozoic represents a unique time in the evolution of the Earth's atmosphere and ocean redox conditions. At that time, there were oxygenated surface waters but copious amounts of reduced iron episodically supplied from hydrothermal sources upwelled onto large areas of continental shelves from the deep anoxic waters. A dynamic shallow-water redoxcline in an iron-rich ocean would have provided an ideal environment for the proliferation of microaerophilic, chemolithotrophic microbial ecosystems. Until the rise of atmospheric oxygen at 2.32 Ga (Bekker et al., 2004), a shallow-water redoxcline was likely absent in the anoxic oceans, while after ca. 1.7 Ga, the deep ocean became Fe-poor due to either euxinic or suboxic deep-water conditions (Poulton et al., 2004; Slack et al., 2007). The absence of true negative Ce anomalies on several Archean carbonate platforms is consistent with reducing shallow-water conditions in the Archean oceans (e.g. Kamber and Webb, 2001). The deep oceans were likely fully ventilated in the Neoproterozoic, restricting iron-oxidizing bacteria to shallow-water environments with localized terrestrially-derived iron fluxes (e.g. Dahanayake and Krumbein, 1986) or to areas with enhanced local hydrothermal activity (e.g. Reysenbach and Cady, 2001). The Animikie Lagerstattën and the biotas preserved in broadly correlative iron formations are therefore related to unique environmental conditions when a dynamic chemocline allowed for the proliferation of iron-oxidizing bacteria. Global-scale ocean redox evolution linked with tectonomagmatic events provides an explanation for the apparently temporally restricted but geographically extensive distribution of the Gunflint biota.

6. Conclusions

A detailed geochemical and petrographic examination of the Animikie basin iron formations allowed reconstruction of basin redox and ecosystem structure. We found a progressive change in Ce anomalies in a transect from deep- to shallow-water facies in the Animikie basin revealing the presence of a basin-wide redoxcline. Iron oxide-rich siliceous stromatolites and samples of iron formation lack negative Ce anomalies, which contrasts with shallower-water, tidally-influenced, Mn-rich microbialites containing significant negative Ce anomalies. This trend in Ce anomalies indicates that the siliceous stromatolites formed in low oxygen conditions at or near the redoxcline. Low oxygen conditions provided the ideal setting for the proliferation of chemolithotrophic iron-oxidizing bacteria, consistent with interpretations of distinctive microfossils in Gunflint stromatolites.

Iron isotopes provided a means to trace local redox conditions and a way to distinguish between oxygenic photosynthetic or iron-oxidizing benthic microbial communities. Considering that high levels of oxygen found in modern photosynthetically-active cyanobacterial mats result in quantitative ferrous iron oxidation, iron-oxides precipitated in cyanobacterial mats are expected to have the same δ^{56}Fe values as the dissolved iron sources. In contrast, we observed a predominance of positive δ^{56}Fe values in the stromatolites, which indicates modest extent of oxidation and directly contradicts cyanobacterial interpretation of the studied microbial ecosystems.

The benthic ecosystems forming the Gunflint stromatolites induced low degrees of iron oxidation under suboxic conditions and in cases contain microfossils with morphologies suggestive of iron-oxidizing bacteria (e.g. Knoll, 2003). Combined, the geochemical and paleontological data provide compelling evidence for chemolithotrophic, iron-oxidizing microbial ecosystems in the Animikie basin. Stromatolites with evidence for chemolithotrophic ecosystem can be traced for over 100 km along the margin of the Superior craton and are found in nearly coeval iron formations from several other cratons. The Animikie-type stromatolites and microfossils had a widespread spatial but an apparently restricted temporal distribution, likely reflecting an ecosystem response to a period of unique ocean redox conditions. In the late Paleoproterozoic when surface waters were already fully oxygenated, reductants supplied by hydrothermal sources episodically overwhelmed deep-ocean redox state allowing for delivery of hydrothermally dominated seawater onto large areas of continental shelves where iron formations were deposited. The presence of this dynamic shallow-water redoxcline separating iron-rich deep waters from fully oxygenated shallow-waters likely provided an ideal setting for the proliferation of microaerophilic, chemolithotrophic microbial ecosystems.

Acknowledgements

NP would like to thank Marcia Bjornerud for several reviews of earlier drafts and continuous guidance, Balz Kamber for review of an earlier draft and sample analysis and Andy Knoll for access to the Harvard paleontological collection; RS and NP would like to thank Cleveland Cliffs Mining, Cliffs-Erie, and the Minnesota Department of Natural Resources for access to mines and core samples; NP acknowledges funding from WHOI Summer Student Fellowship program, NSF Graduate Research Fellowship, and Lawrence University Excellence in Science Fund; AB from the NSF grant EAR-05-45484, NASA Astrobiology Institute award No. NNA04CC09A, NSERC Discovery Grant, and TGI-3 program operated by the Geological Survey of Canada; and OR from the OCE-0647948, OCE-0550066 and Frank and Lisina Hoch Endowed Fund.

Appendix A. Supplementary data

Supplementary data associated with this article can be found, in the online version, at doi:10.1016/j.cbpb.2009.06.012.

Appendix B

Appendix A. The latitude and longitude of and references describing the localities sampled for this study.

Appendix B. Major element and REE concentrations. *Denotes samples duplicated at Activation Laboratories Ltd. (Ancaster, Ontario). Facies type abbreviations are: CIF, Cherty iron-formation, HRS, Hematite-rich stromatolites, MRS, Microfossil-rich stromatolites, MnRM, Mn-rich microbialites, SIF, Slaty iron-formation. See main text for facies details.

Appendix C. Sample description, and trace element and REE concentrations for samples from LWD-99-2 drill core shown in main text Fig. 6. Facies type abbreviations are: CIF, Cherty iron-formation, HRS, Hematite-rich stromatolites, MRS, Microfossil-rich stromatolites, MnRM, Mn-rich microbialites, SIF, Slaty iron-formation. See main text for facies details.

Appendix References

[1] Severson, M., 2005. Preliminary Correlations in the Biwabik iron formation in the Virginia Horn Area, NRRI/MAP-2005/01, National Resources Research Institute Duluth.

[2] Pufahl, P.K., Stratigraphic architecture of a Palaeoproterozoic Iron Formation, unpublished Master's thesis, Lakehead University.

[3] Fralick, P.W., Pufahl, P.K., 2000, Field Guide for the 46th annual Institute on Lake Superior Geology, Institute on Lake Superior Geology, Thunder Bay, ON.

[4] Cloud, P.E., Significance of Gunflint (Precambrian) Microflora. Science, 148, 27–35.

[5] Hofmann, H., 1969, Stromatolites from the Proterozoic Animikie and Sibley Groups. Geological Survey of Canada Paper, Geological Survey of Canada, 1969, p. 68.

[6] Han, T.M., Runnegar, B., 1992, Megascopic eukaryotic algae from the 2.1-billion-year-old Negaunee Iron-Formation, Michigan, Science, 257, 232–235.

[7] Bayley, R. W., Dutton, C. E., Lamey, C. A., Treves, S. B., 1966, Geology of the Menominee iron-bearing district Dickinson County, Michigan and Florence and Marinette Counties, Wisconsin. USGS Prof. Paper 513 pp. 96.

References

Amard, B., Bertrand Sarfati, J., 1997. Microfossils in 2000 Ma old cherty stromatolites of the Franceville Group, Gabon. Precambrian Res. 81, 197–221.

Anbar, A.D., Rouxel, O., 2007. Metal stable isotopes in paleoceanography. Annu. Rev. Earth Planet. Sci. 35, 717–746.

Awramik, S.M., Barghoorn, E.S., 1977. Gunflint microbiota. Precambrian Res. 5, 121–142.

Balci, N., Bullen, T.D., Witte-Lien, K., Shanks, W.C., Motelica, M., Mandernack, K.W., 2006. Iron isotope fractionation during microbially stimulated Fe(II) oxidation and Fe(III) precipitation. Geochim. Cosmochim. Acta 70, 622–639.

Baragar, W., Scoates, F., 1981. The Circum-Superior belt: a Proterozoic plate margin? In: Kröner, A. (Ed.), Precambrian Plate Tectonics. InElsevier, Amsterdam, pp. 295–330.

Barghoorn, E.S., Tyler, S.A., 1965. Microorganisms from the Gunflint Chert. Science 147, 563–575.

Barrett, J., Jarvis, I., 1988. Rare-earth element geochemistry of metalliferous sediments from DSDP Leg 92. the East Pacific Rise transect. Chem. Geol. 67, 243–259.

Bau, M., 1993. Effects of syn-depositional and postdepositional processes on the rare-earth element distribution in Precambrian iron-formations. Eur. J. Mineral. 5, 257–267.

Bau, M., 1999. Scavenging of dissolved yttrium and rare earths by precipitating iron oxyhydroxide: experimental evidence for Ce oxidation, Y–Ho fractionation, and lanthanide tetrad effect. Geochim. Cosmochim. Acta 63, 67–77.

Bau, M., Dulski, P., 1996. Distribution of yttrium and rare-earth elements in the Penge and Kuruman Iron-Formations, Transvaal Supergroup, South Africa. Precambrian Res. 79, 37–55.

Beard, B.L., Johnson, C.M., VonDamm, K.L., Poulson, R.L., 2003. Iron isotope constraints on Fe cycling and mass balance in oxygenated Earth oceans. Geology 31, 629–632.

Bekker, A., Holland, H.D., Wang, P.L., Rumble, D., Stein, H.J., Hannah, J.L., Coetzee, L.L., Beukes, N.J., 2004. Dating the rise of atmospheric oxygen. Nature 427, 117–120.

Brotton, S.J., Shapiro, R., van der Laan, G., Guo, J., Glans, P.A., Ajello, J.M., 2007. Valence state fossils in Proterozoic stromatolites by L-edge X-ray absorption spectroscopy. J. Geophys. Res.-Biogeosci. 112, G03004.1–G03004.11.

Bullen, T.D., White, A.F., Childs, C.W., Vivit, D.V., Schulz, M.S., 2001. Demonstration of significant abiotic iron isotope fractionation in nature. Geology 29, 699–702.

Byrne, R., Sholkovitz, E., 1996. Marine chemistry and geochemistry of the lanthanides. In: GschneiderJr. Jr., K.A., Eyring, L. (Eds.), Handbook on the Physics and Chemistry of the Rare Earths, vol. 23. Elsevier, Amsterdam, pp. 497–593.

Canfield, D.E., Rosing, M.T., Bjerrum, C., 2006. Early anaerobic metabolisms. Philos. Trans. R. Soc., B 361, 1819–1836.

Chu, N.-C., Johnson, C.M., Beard, B.L., German, C.R., Nesbitt, R.W., Frank, M., Bohn, M., Kubik, P. W., Usui, A., Graham, I., 2006. Evidence for hydrothermal venting in Fe isotope compositions of the deep Pacific Ocean through time. Earth Planet. Sci. Lett. 245, 202–217.

Cloud, P.E., 1965. Significance of Gunflint (Precambrian) Microflora. Science 148, 27–35.

Croal, L.R., Johnson, C.M., Beard, B.L., Newman, D.K., 2004. Iron isotope fractionation by Fe (II)-oxidizing photoautotrophic bacteria. Geochim. Cosmochim. Acta 68, 1227–1242.

Dahanayake, K., Krumbein, W.E., 1986. Microbial structures in oolitic iron formations. Miner. Depos. 21, 85–94.

Dauphas, N., Cates, N.L., Mojzsis, S.J., Busigny, V., 2007. Identification of chemical sedimentary protoliths using iron isotopes in the >3750 Ma Nuvvuagittuq supracrustal belt, Canada. Earth Planet. Sci. Lett. 254, 358–376.

Dauphas, N., vanZuilen, M., Wadhwa, M., Davis, A.M., Marty, B., Janney, P.E., 2004. Clues from Fe isotope variations on the origin of early Archean BIFs from Greenland. Science 306, 2077–2080.

Eggins, S.M., Woodhead, J.D., Kinsley, L.P.J., Mortimer, G.E., Sylvester, P., McCulloch, M.T., Hergt, J.M., Handler, M.R., 1997. A simple method for the precise determination of 40 trace elements in geological samples by ICPMS using enriched isotope internal standardization. Chem. Geol. 134, 311–326.

Emerson, D., Moyer, C., 1997. Isolation and characterization of novel iron-oxidizing bacteria that grow at circumneutral pH. Appl. Environ. Microbiol. 63, 4784–4792.

Emerson, D., Revsbech, N.P., 1994. Investigation of an iron-oxidizing microbial mat community located near Aarhus, Denmark — field studies. Appl. Environ. Microbiol. 60, 4022–4031.

Fralick, P., 1989. Microbial bioherms, Lower Proterozoic Gunflint Formation, Thunder Bay, Ontario. In: Geldsetzer, H.H.J., James, N.P., Tebbutt, G.E. (Eds.), Reefs: Canada and adjacent areas. In: Memoirs. Canadian Society of Petroleum Geologists, pp. 24–29.

Fralick, P., Davis, D.W., Kissin, S.A., 2002. The age of the Gunflint Formation, Ontario, Canada: single zircon U–Pb age determinations from reworked volcanic ash. Can. J. Earth Sci. 39, s1085–1091.

French, B.V., 1973. Mineral assemblages in diagenetic and low-grade metamorphic iron-formation. Economic Geology 68, 1063–1074.

French, J.E., Heaman, L.M., Chacko, T., Srivastava, R.K., 2008. 1891–1883 Ma Southern Bastar-Cuddapah mafic igneous events, India. A newly recognized large igneous province: Precambrian Research 160, 308–322.

German, C.R., Elderfield, H., 1990. Application of the Ce-anomaly as a paleoredox indicator: the ground rules. Paleoceanography 5, 823–833.

German, C.R., Holliday, B.P., Elderfield, H., 1991. Redox cycling of rare earth elements in the suboxic zone of the Black Sea. Geochim. Cosmochim. Acta 55, 3553–3558.

Golubic, S., Lee, S.J., 1999. Early cyanobacterial fossil record: preservation, palaeoenvironments and identification. European Journal of Phycology 34, 339–348.

Govindaraju, K., 1994. Compilation of working values and sample description for 383 geostandards. Geostandards Newsletter 18, 1–158.

Gross, G.A., 1972. Primary features in cherty iron-formations. Sed. Geol. 7, 241–261.

Halls, H.C., Heaman, L.M., 2000. The paleomagnetic significance of new U–Pb age data from the Molson dyke swarm, Cauchon Lake area, Manitoba. Can. J. Earth Sci. 37, 957–966.

Heaman, L.M., Machado, N., Krogh, T.E., Weber, W., 1986. Precise U–Pb Zircon Ages for the Molson Dyke Swarm and the Fox River Sill — constraints for Early Proterozoic Crustal Evolution in Northeastern Manitoba, Canada. Contrib. Mineral. Petrol. 94, 82–89.

Heaman, L.M., Peck, D., Toope, K., 2009. Timing and geochemistry of 1.88 Ga Molson Igneous Events, Manitoba: Insights into the formation of a craton-scale magmatic and metallogenic province. Precambrian Res. 172 (1–2), 143–162.

Hoffman, P.F., 1987. Early Proterozoic foredeeps, foredeep magmatism, and Superior-type iron-formations of the Canadian Shield. in Proterozoic Lithospheric Evolution (ed. Kroner, A.) joint American Geophysical Union, Washington D.C., and Geological Society of America, Boulder, publication. pg. 85-98.

Hofmann, H., 1969. Stromatolites from the Proterozoic Animikie and Sibley Groups. Geological Survey of Canada Paper, Geological Survey of Canada. pp. 68.

Holland, H.D., 1984. The chemical evolution of the atmosphere and oceans. NJ, Princeton University Press. pp. 598.

Johnson, C., Beard, B., 2006. Fe isotopes: an emerging technique in understanding modern and ancient biogeochemical cycles. GSA Today 16, 4–10.

Johnson, C.M., Beard, B.L., Beukes, N.J., Klein, C., O'Leary, J.M., 2003. Ancient geochemical cycling in the Earth as inferred from Fe isotope studies of banded iron formations from the Transvaal Craton. Contrib. Mineral. Petrol. 144, 523–547.

Johnson, C.M., Beard, B.L., Klein, C., Beukes, N.J., Roden, E.E., 2008. Iron isotopes constrain biologic and abiologic processes in banded iron formation genesis. Geochim. Cosmochim. Acta 72, 151–169.

Jorgensen, B.B., Revsbech, N.P., Cohen, Y., 1983. Photosynthesis and structure of Benthic Microbial Mats — microelectrode and SEM studies of 4 cyanobacterial communities. Limnol. Oceanogr. 28, 1075–1093.

Kamber, B.S., 2009. Geochemical fingerprinting: 40 years of analytical development and real world applications. Appl. Geochem. 24 (6), 1074–1086.

Kamber, B.S., Bolhar, R., Webb, G.E., 2004. Geochemistry of late Archaean stromatolites from Zimbabwe: evidence for microbial life in restricted epicontinental seas. Precambrian Res. 132, 379–399.

Kamber, B.S., Webb, G.E., 2001. The geochemistry of late Archaean microbial carbonate: Implications for ocean chemistry and continental erosion history. Geochim. Cosmochim. Acta 65, 2509–2525.
Kappler, A., Pasquero, C., Konhauser, K.O., Newman, D.K., 2005. Deposition of banded iron formations by anoxygenic phototrophic Fe(II)-oxidizing bacteria. Geology 33, 865–868.
Knoll, A.H., 2003. Life on a young planet: the first three billion years of evolution on earth. NJ, Princeton University Press. pp. 304.
Knoll, A.H., Barghoorn, E.S., 1976. Gunflint-type microbiota from Duck Creek Dolomite, Western-Australia. Orig. Life Evol. Biosph. 7, 417–423.
Knoll, A.H., Simonson, B., 1981. Early Proterozoic Microfossils and Penecontemporaneous Quartz Cementation in the Sokoman Iron Formation, Canada. Science. 211, 478–480.
Knoll, A.H., Strother, P.K., Rossi, S., 1988. Distribution and diagenesis of Microfossils from the Lower Proterozoic Duck Creek Dolomite, Western-Australia. Precambrian Res. 38, 257–279.
Konhauser, K.O., Hamade, T., Raiswell, R., Morris, R.C., Ferris, F.G., Southam, G., Canfield, D.E., 2002. Could bacteria have formed the Precambrian banded iron formations? Geology 30, 1079–1082.
Lager, I., 2001. The geology of the Palaeoproterozoic limestone-hosted Dannemora iron deposit, Sweden. SGU rapporter och meddelanden, vol. 107, p. 49-49.
Levasseur, S., Frank, M., Hein, J.R., Halliday, A.N., 2004. The global variation in the iron isotope composition of marine hydrogenetic ferromanganese deposits: implications for seawater chemistry? Earth Planet. Sci. Lett. 224, 91–105.
Maliva, R.G., Knoll, A.H., Simonson, B.M., 2005. Secular change in the Precambrian silica cycle: insights from chert petrology. Geol. Soc. Am. Bull. 117, 835–845.
Morey, G.B., Southwick, D.L., 1993. Stratigraphic and sedimentological factors controlling the distribution of epigenetic manganese deposits in iron-formation of the Emily District, Cuyuna Iron Range, East-Central Minnesota. Economic Geology and the Bulletin of the Society of Economic Geologists 88, 104–122.
Nance, W.B., Taylor, S.R., 1976. Rare earth patterns and crustal evolution: I. Australian post-Archean sedimentary rocks, Geochimica et Cosmochimica Acta 40, 1539–1551.
Ohta, A., Kawabe, I., 2001. REE(III) adsorption onto Mn dioxide (delta-MnO2) and Fe oxyhydroxide: Ce(III) oxidation by delta-MnO2. Geochim. Cosmochim. Acta 65, 695–703.
Ojakangas, R.W., 1983. Test article sample title placed here. America Memoir, Geological Society of America. 49–66.
Ojakangas, R.W., Morey, G.B., Southwick, D.L., 2001. Paleoproterozoic basin development and sedimentation in the Lake Superior region, North America. Sed. Geol. 141, 319–341.
Poulton, S.W., Fralick, P.W., Canfield, D.E., 2004. The transition to a sulphidic ocean 1.84 billion years ago. Nature. 431, 173–177.
Pufahl, P.K., Fralick, P.W., 2004. Depositional controls on Palaeoproterozoic iron formation accumulation, Gogebic Range, Lake Superior region, USA. Sedimentology 51, 791–808.
Reysenbach, A., Cady, S., 2001. Microbiology of ancient and modern hydrothermal systems. Trends Microbiol. 9, 79–86.
Rouxel, O., Bekker, A., Edwards, K., 2005. Iron isotope constraints on the Archean and Paleoproterozoic Ocean redox state. Science. 307, 1088–1091.
Rouxel, O., Shanks, W.C., Bach, W., Edwards, K., 2008b. Integrated Fe and S isotope study of seafloor hydrothermal vents at East Pacific Rise 9-10 N. Chem. Geol. 252, 214–227.
Rouxel, O., Sholkovitz, E., Charette, M., Edwards, K., 2008a. Iron isotope fractionation in Subterranean Estuaries. Geochim. Cosmochim. Acta 72, 3413–3430.
Rouxel, O.J., Edwards, K.J., Moyer, C.L., Wheat, G., 2007. Biogeochemical cycling of iron isotopes at Loihi Seamount. Eos Transactions 88, 52-52.
Schneider, D.A., Bickford, M.E., Cannon, W.F., Schulz, K.J., Hamilton, M.A., 2002. Age of volcanic rocks and syndepositional iron formations, Marquette Range Supergroup: implications for the tectonic setting of Paleoproterozoic, iron formations of the Lake Superior region. Can. J. Earth Sci. 39, 999–1012.
Schulz, K.J., Cannon, W.F., 2007. The penokean orogeny in the lake superior region: Precambrian Research 157, 4–25.
Severmann, S., Johnson, C.M., Beard, B.L., German, C.R., Edmonds, H.N., Chiba, H., Green, D.R. H., 2004a. The effect of plume processes on the Fe isotope composition of hydrothermally derived Fe in the deep ocean as inferred from the Rainbow vent site, Mid-Atlantic Ridge, 36 14 N. Earth Planet. Sci. Lett. 225, 63–76.
Severmann, S., Johnson, C.M., Beard, B.L., McManus, J., 2006. The effect of early diagenesis on the Fe isotope compositions of porewaters and authigenic minerals in continental margin sediments. Geochim. Cosmochim. Acta 70, 2006–2022.
Severmann, S., Johnson, C.M., Beard, B.L., Yvennes, M., Huerta-Diaz, M.A., Thamdrup, B., Hoehler, T., Welch, S., 2004b. Fe and S isotope variations in cyanobacterial mats: modern analogues of ancient stromatolites. EOS Transactions 85, 47.
Sharma, M., Polizzotto, M., Anbar, A.D., 2001. Iron isotopes in hot springs along the Juan de Fuca Ridge. Earth and Planetary Sciences Letters 194, 39–51.
Slack, J.F., Grenne, T., Bekker, A., Rouxel, O.J., Lindberg, P.A., 2007. Suboxic deep seawater in the late Paleoproterozoic: evidence from hematitic chert and iron formation related to seafloor-hydrothermal sulfide deposits, central Arizona, USA. Earth Planet. Sci. Lett. 255, 243–256.
Sommers, M.G., Awramik, S.M., Woo, K.S., 2000. Evidence for initial calcite-aragonite composition of Lower Algal Chert Member ooids and stromatolites, Paleoproterozoic Gunflint Formation, Ontario, Canada. Can. J. Earth Sci. 37, 1229–1243.
Staubwasser, M., Blanckenburg, F.V., Schoenberg, R., 2006. Iron isotopes in the early marine diagenetic iron cycle. Geology 34, 629–632.
Strother, P.K., Tobin, K., 1987. Observations on the Genus *Huroniospora* Barghoorn-Implications for Paleoecology of the Gunflint Microbiota. Precambrian Res. 36, 323–333.
Tazaki, K., Ferris, F.G., Wiese, R.G., Fyfe, W.S., 1992. Iron and graphite associated with fossil bacteria in chert. Chem. Geol. 95, 313–325.
Trouwborst, R.E., Johnston, A., Koch, G., Pierson, B.K., 2007. Biogeochemistry of Fe(II) oxidation in a photosynthetic microbial mat: implications for Precambrian Fe(II) oxidation. Geochim. Cosmochim. Acta 71, 4629–4643.
Walter, M.R., Goode, A.D.T., Hall, W.D.M., 1976. Microfossils from a newly discovered Precambrian Stromatolitic Iron Formation in Western-Australia. Nature. 261, 221–223.
Widdel, F., Schnell, S., Heising, S., Ehrenreich, A., Assmus, B., Schink, B., 1993. Ferrous iron oxidation by anoxygenic phototrophic bacteria. Nature. 362, 834–836.
Yongding, D., Haiming, S., Jiying, S., 2004. Fossil bacteria in Xuanlong iron ore deposits of Hebei Province. Science in China (Earth Sciences 47, 347–356.
Zhu, X.K., O'Nions, R.K., Guo, Y., Reynolds, B.C., 2000. Secular variation of iron isotopes in North Atlantic deep water. Science. 287, 2000–2002.
Zielinski, A.M., Manusco, J.J., Frizado, J.P., Waidler, R.J., 1994. Manganese-rich oncolites in the Biwabik iron formation, Eveleth mine, Mesabi North Range, Short communications to the Geological Survey of Minnesota, pp. 48–59.